Preprint typeset in JHEP style. - PAPER VERSION

Cavendish–HEP–05/24
GEF–TH–12/2005
ITP–UU–05/57
NIKHEF/2005–026

Single-top production in MC@NLO

Stefano Frixione

INFN, Sezione di Genova, Via Dodecaneso 33, 16146 Genova, Italy
E-mail: Stefano.Frixione@cern.ch

Eric Laenen

NIKHEF, Kruislaan 409, 1098 SJ Amsterdam, The Netherlands and Institute for Theoretical Physics, Utrecht University, Leuvenlaan 4, 3584 CE Utrecht, The Netherlands
E-mail: Eric.Laenen@nikhef.nl

Patrick Motylinski

NIKHEF, Kruislaan 409, 1098 SJ Amsterdam, The Netherlands
E-mail: patrickm@nikhef.nl

Bryan R. Webber

Cavendish Laboratory, J.J. Thompson Avenue, Cambridge CB3 0HE, U.K.
E-mail: webber@hep.phy.cam.ac.uk

ABSTRACT: We match next-to-leading order QCD results for single-top hadroproduction with parton shower Monte Carlo simulations, according to the prescription of the MC@NLO formalism. In this way, we achieve the first practical implementation in MC@NLO of a process that has both initial- and final-state collinear singularities. We show that no difficulties of principle arise from this complication, and present selected results relevant to the Tevatron.

KEYWORDS: QCD, Monte Carlo, NLO Computations, Resummation, Collider Physics, Heavy Quarks.

Contents

1. Introduction **1**

2. Single-top cross sections **3**
2.1 NLO computation 3
2.1.1 Matrix elements 4
2.1.2 Subtraction procedure 5
2.2 MC cross sections expanded to NLO 10

3. MC@NLO **13**

4. Results **16**

5. Conclusions **22**

A. Kinematics **23**

B. MC subtraction terms **26**

1. Introduction

Heavy flavour production at hadron colliders has been the subject of extensive theoretical and experimental studies for more than twenty years. The discovery of the top quark has offered an excellent opportunity to test QCD predictions much more reliably than in the case of bottom or charm, thanks to the smaller value of $\alpha_{\rm S}$ and the relatively minor impact of long-distance effects, the top having no time to hadronize before decay. At present, all comparisons between theory and data concern $t\bar{t}$ pair production; a crucial role in the satisfactory agreement between predictions and experimental results is played by the next-to-leading order (NLO) QCD corrections [1, 2, 3, 4], which enlarge the leading-order cross section by about 30% at the Tevatron. A companion process to pair production is that in which a single top quark is present in the final state. In such a case, a weak-interaction Wtb vertex is involved, and thus the single-t cross section is smaller than the one for $t\bar{t}$ (in spite of being favoured by phase space volume), which so far has prevented observation of such a production mechanism by Tevatron experiments. In terms of Standard Model physics, single-t production is a direct probe of the weak interactions of the top, which in fact constitutes the main interest of single-t signals. Amongst other things, this may lead to measurements that have not been performed so far, namely of the CKM matrix element V_{tb}, and of the b parton density. Single-t production is in addition an important background for many searches for new physics, and can in general be seen as an effective way to study new physics phenomena in the heavy sector.

For single-t searches, or counting experiments in which single-t is a background, it is crucial to have a reliable estimate of the number of events expected, i.e. of the total rate. In this respect, NLO results are mandatory, also in view of the fact that they allow a sensible assessment of the size of unknown contributions of higher orders. Calculations of fully-differential NLO single-t cross sections have been performed in refs. [5, 6, 7, 8] and, including NLO top quark decay, in refs. [9, 10, 11, 12, 13]. On the other hand, in order to optimize acceptance cuts in an experimental analysis, or to perform full detector simulations, one needs realistic hadron-level events, which are obtained with Monte Carlo event generators that incorporate the simulation of parton showers and hadronization models.

The complementary benefits of fixed-order computations and parton shower simulations have been discussed at length in the literature, as well as the advantages of combining them into a framework which would retain the strong points of each of them. The MC@NLO approach [14, 15] (we shall refer to these papers as to **I** and **II** respectively hereafter) provides a way of achieving this, by allowing one to match cross sections computed at NLO in QCD with an event generator. No modifications to the latter are necessary, and therefore *existing* parton shower Monte Carlos can be used for this purpose.

Although the MC@NLO formalism has been defined in full generality in **I**, explicit implementation details have been given there only for processes with no final-state QCD emissions at the level of hard reactions. Such a case has been considered later in **II**, with the implementation of $t\bar{t}$ and of $b\bar{b}$ production. In the context of MC@NLO, a *process-independent* calculation is required for each type of soft and/or collinear singularity which appears in the NLO real matrix elements. A quick inspection of the processes implemented so far (see ref. [16]) should convince the reader that the *only* singularity structure untreated is the final-state collinear one. We shall deal with this singularity in the present paper. It must be clear that, as for all of the other singularities which have been studied previously, our formulation will not depend on the fact that the specific single-t production process is considered here: in the derivation of the analytical formulae the nature of the hard reaction is irrelevant (which is further evidenced by the fact that the inclusion of single-t production in MC@NLO relies significantly on results obtained in **I** and **II**). What we achieve here is therefore, besides the addition of an important process to the MC@NLO framework, the capability of including other processes in MC@NLO without the need of performing further analytical computations, notably those having final-state (massless) partons at lowest order.

The paper is organized as follows: in sect. 2 we discuss single-t production in the context of fixed-order computations and Monte Carlo simulations. Sect. 2.1.1 reviews the status of the matrix elements used in the present computation. We limit ourselves here to implementing the s- and t-channel production mechanisms, and neglect spin correlations in production. In sect. 2.1.2 we show that some changes can be made in the subtraction formalism [17, 18] upon which MC@NLO is based, which leave its analytical expression unaffected, but improve its numerical stability. We then proceed to sect. 2.2, where we write down the approximate single-t production cross sections generated by HERWIG, which enter the definition of the MC subtraction terms needed for the matching with NLO results. Implementation details of MC@NLO, concerning in particular the simultaneous presence of initial- and final-state collinear singularities, are given in sect. 3. We present results for single-t production at the Tevatron in sect. 4; phenomenological studies, including results for the LHC, will be the subject of a future paper. Finally, conclusions and future prospects are reported in sect. 5. Some technical details are collected in the Appendices.

2. Single-top cross sections

Each process in MC@NLO is based on two main building blocks: a fully-exclusive NLO computation; and the knowledge of the so-called MC subtraction terms, which are closely related to the first non-trivial order in the formal $\alpha_{\rm S}$ expansion of the HERWIG Monte Carlo result. We shall treat these two issues in turn.

2.1 NLO computation

Fully-exclusive observable predictions do not strictly exist in QCD: the theory has finite resolution power, in the sense defined by the KLN theorem. However, we can conventionally talk of fully-exclusive computations, as those in which the cancellation of the infrared singularities is *formally* achieved analytically in an observable-independent manner, and the four-momenta of all of the final-state partons are available for defining the observables – this does not violate the KLN theorem, since the formal cancellation mentioned above actually occurs only in the case of infrared-safe observables. Fully-exclusive computations are crucial for the matching of NLO cross sections with Monte Carlos, since the latter need to know the four-momenta of all the particles involved in the hard process in order to compute the initial conditions and the various branching probabilities for the parton showers. Modern computations of this kind are based on universal subtraction or slicing formalisms; we shall discuss the one used within MC@NLO in sect. 2.1.2. Before doing that, we give some details specific to the matrix elements for single-t production.

2.1.1 Matrix elements

The lowest-order parton level processes are customarily divided into three classes that will also serve to categorize the NLO contributions. They are shown in fig. 1. In the first diagram the single top quark is produced in the annihilation process

$$u + \bar{d} \rightarrow t + \bar{b}\,, \tag{2.1}$$

via a time-like W boson, and is therefore called the s-channel process. In the second diagram, the initial bottom quark is converted into a top quark via the exchange of a W-boson

$$b + u \rightarrow t + d\,, \tag{2.2}$$

and is therefore called the t-channel process. The final two graphs represent the Wt process in which the top quark is produced in association with a real W

$$b + g \rightarrow W + t\,. \tag{2.3}$$

The cross section for this process occurring at the Tevatron is very small and we neglect it in this paper. For the LHC this process becomes non-negligible however. Note that in reactions (2.1) and (2.2) we have only listed the CKM-dominant combinations of quark flavours, but all CKM-allowed combinations are included in this paper. Consistently, the b quark is always assumed to be massless.

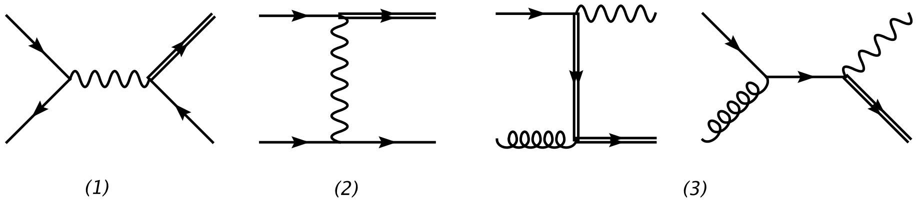

Figure 1: Leading order diagrams for single-t production in the (1) s-channel, (2) t-channel and (3) Wt-mode. The t-quark line is doubled.

In NLO one must include virtual and real corrections to the s- and t-channel processes. The virtual corrections consist of vertex corrections to diagrams *(1)* and *(2)* in fig. 1, together with the self-energy corrections to the t-quark line[1]. We shall not discuss these corrections in detail, nor give their explicit expressions, as these are already given in the literature. To prepare a remark on single-antitop production further below, we recall here that the vertex correction in the first diagram of fig. 2 is proportional to the lowest order vertex $\gamma^\mu(1-\gamma_5)$ because only light quark lines are attached to it. If the top quark line is attached as in the second diagram of fig. 2, a second form factor appears at NLO, proportional to the difference $(p_t^\mu - p_{\bar{b}}^\mu)/m_t$. A similar situation occurs in the t-channel.

[1]Box graphs vanish since they involve a single colour matrix on a fermion line, i.e. a null trace.

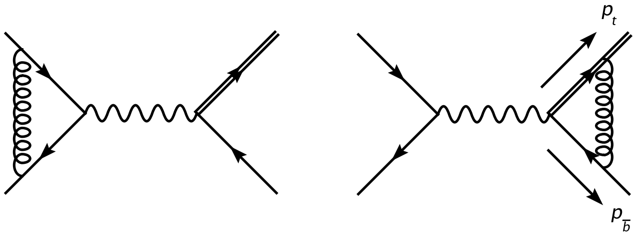

Figure 2: Virtual vertex corrections to s-channel single-t production.

Concerning the real-emission corrections, we categorize these processes by the dominant CKM contributions, as follows

$$u\bar{d} \longrightarrow t\bar{b}g\,, \tag{2.4}$$

$$ub \longrightarrow tdg\,, \tag{2.5}$$

$$b\bar{d} \longrightarrow t\bar{u}g\,, \tag{2.6}$$

$$ug \longrightarrow t\bar{b}d\,, \tag{2.7}$$

$$\bar{d}g \longrightarrow t\bar{b}\bar{u}\,, \tag{2.8}$$

$$bg \longrightarrow td\bar{u}\,. \tag{2.9}$$

A rather detailed discussion of these processes, and how they are assigned to s- and t-channel, can be found in the next section.

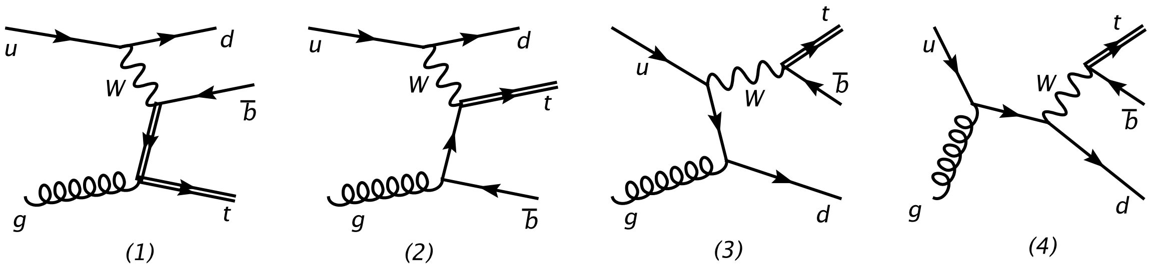

Figure 3: Diagrams contributing to $ug \to t\bar{b}d$.

The calculation of the single-$\bar{t}$ cross section is perfectly similar to that for the single-t described above, after charge conjugation. It may be perhaps less apparent that the second vertex form factor, mentioned above, proportional to $(p_{\bar{t}} - p_b)/m_t$ remains unchanged, since the quark propagators change the sign of the mass term. However the charge flow of the conjugated amplitude is also reversed, resulting in an unchanged expression.

2.1.2 Subtraction procedure

In order to implement a process in MC@NLO, its NLO cross section must be computed according to the subtraction formalism presented in refs. [17, 18] (denoted as

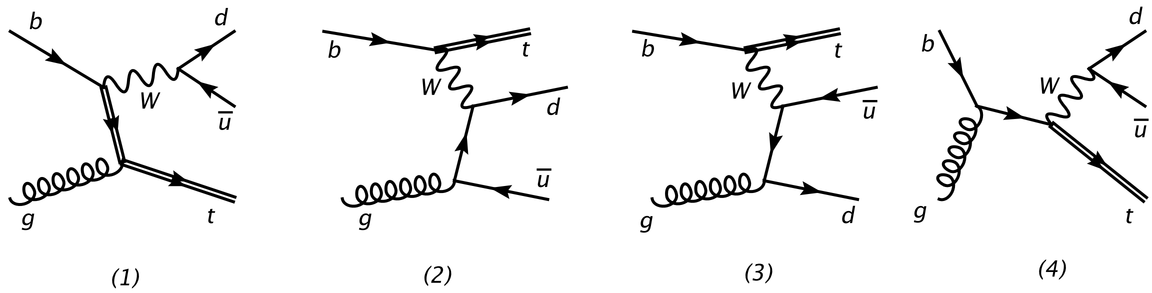

Figure 4: Diagrams contributing to $bg \to td\bar{u}$.

FKS henceforth). The basic idea in FKS is that of partitioning the phase space of the final-state partons involved in real-emission contributions, in such a way that the resulting regions do not overlap, cover the whole phase space, and each of them contains at most one collinear and one soft singularity. In each of these regions it is natural to select the one parton (called the FKS parton here) with which the singularities are associated. Denoting by $\mathcal{M}^{(r)}$ the generic real matrix elements, this amounts to writing[2]

$$1 = \sum_i \mathcal{S}_i^{(0)} + \sum_{ij} \mathcal{S}_{ij}^{(1)}\,, \tag{2.10}$$

$$\mathcal{M}^{(r)} = \sum_i \mathcal{S}_i^{(0)} \mathcal{M}^{(r)} + \sum_{ij} \mathcal{S}_{ij}^{(1)} \mathcal{M}^{(r)}\,. \tag{2.11}$$

The FKS parton is labelled with i in eqs. (2.10) and (2.11). The first term on the r.h.s. of eq. (2.11) gives a divergent contribution (i.e., a contribution which has to be subtracted) only in the infrared regions in which parton i is soft and/or collinear to one of the initial-state partons. Analogously, the only infrared regions in which the second term on the r.h.s. of eq. (2.11) is divergent are those in which parton i is soft and/or collinear to final-state parton j. More precisely, denoting by p_α and k_α the four-momenta of the initial- and final-state particles respectively, we have

$$\lim_{k_i^0 \to 0} \left(\mathcal{S}_i^{(0)} + \sum_j \mathcal{S}_{ij}^{(1)} \right) = 1\,, \tag{2.12}$$

$$\lim_{\vec{k}_i \parallel \vec{p}_1} \mathcal{S}_i^{(0)} = 1\,, \tag{2.13}$$

$$\lim_{\vec{k}_i \parallel \vec{p}_2} \mathcal{S}_i^{(0)} = 1\,, \tag{2.14}$$

$$\lim_{\vec{k}_i \parallel \vec{k}_j} \mathcal{S}_{ij}^{(1)} = 1\,, \tag{2.15}$$

[2]The notation of refs. [17, 18] has been slightly changed here in order to simplify the discussion. Functions $\mathcal{S}$ of the present paper play the same role as functions Θ in ref. [18].

while all the other infrared limits not explicitly listed above are zero[3]. Eqs. (2.12)–(2.15) are the *only* properties of the $\mathcal{S}$ functions used in the analytical computations of refs. [17, 18]; their actual functional forms away from the infrared limits are only relevant to numerical integrations. It should be stressed that all partons in the final state may induce a divergence of the real matrix elements; to take this fact into account, the role of FKS parton is given to each parton in turn, which is formally expressed in eq. (2.11) by the sum over i that appears on the r.h.s. there.

After the phase space of the final-state partons is effectively partitioned through eq. (2.11) into different infrared-singular regions, FKS chooses a different phase-space *parametrization* in each of these regions. It must be clear that the phase space is always the same, i.e. that relevant to the n particles involved in real-emission processes; the only difference between the various regions is in the choice of the integration variables which are left after getting rid of the δ functions that appear in the phase-space definition. The integration variables are chosen to perform the necessary analytical integrations in an easy way, and to facilitate importance sampling in numerical integrations. The key variables in the phase-space parametrization associated with $\mathcal{S}_i^{(0)}$ are the energy of parton i (directly related to soft singularities), and the angle between parton i and one of the initial-state partons (directly related to initial-state collinear singularities). For $\mathcal{S}_{ij}^{(1)}$, the energy of parton i and the angle between parton i and parton j (related to a final-state collinear singularity) are chosen instead. Obviously, the indices i and j are dummy here (phase spaces are flavour blind), and therefore there are only two independent functional forms for phase spaces in FKS, which loosely speaking are relevant to initial- and to final-state emissions. More details, and specific functional forms, are given in appendix B.

After the partition of the phase space, achieved by means of $\mathcal{S}_i^{(0)}$ and $\mathcal{S}_{ij}^{(1)}$, it is the matrix elements that determine whether a singularity actually occurs in a given region of such a partition. As a general rule, one should choose the simplest possible forms for the $\mathcal{S}$ functions that still allow subtraction of all singularities. Although this is by no means mandatory (a region without singularities will simply give a finite contribution to the cross section), it is beneficial for well-behaved numerical computations. Since single-t matrix elements have a singularity structure much simpler than that of the matrix elements considered in refs. [17, 18], the $\mathcal{S}$ functions will also be simpler here. We also want to use the present process as a test case, and will define the $\mathcal{S}$'s as smooth functions of invariants, at variance with the original formulation of refs. [17, 18], in which they have been expressed as products of Θ functions.

We start by denoting the four-momenta entering an NLO tree-level single-t pro-

[3]The superscripts (0) and (1) are legacy notation from ref. [17], where these S-functions are related to jet-finding algorithms, and the superscripts indicate the algorithm step at which a merging takes place.

duction process as follows

$$\alpha(p_1) + \beta(p_2) \longrightarrow t(k_1) + \gamma(k_2) + \delta(k_3)\,, \tag{2.16}$$

where α and β are the incoming partons from the left ($p_1^3 > 0$) and from the right ($p_2^3 < 0$) respectively; γ and δ denote light final-state partons. We shall use the following shorthand notation

$$(\alpha, \beta; t, \gamma, \delta) \tag{2.17}$$

for the momentum assignment of eq. (2.16).

We first consider process (2.4); the treatment of processes (2.5) and (2.6) is identical[4]. We assign momenta as follows:

$$(u, \bar{d}; t, \bar{b}, g)\,. \tag{2.18}$$

By inspection of the relevant Feynman diagrams, we immediately conclude that the only singularities are associated with the gluon: the final-state light quark cannot give rise to a collinear divergence, being in all cases connected to a W boson. Therefore, for such processes the gluon will always be the FKS parton and, according to the discussion given at the beginning of this section, we can choose the $\mathcal{S}$ functions in such a way that the only non-zero ones are $\mathcal{S}_3^{(0)}$ and $\mathcal{S}_{32}^{(1)}$. In particular, with the following forms

$$\mathcal{S}_3^{(0)} = \frac{(k_3\cdot k_1)^a (k_3\cdot k_2)^a}{(k_3\cdot k_1)^a (k_3\cdot k_2)^a + (k_3\cdot p_1)^a (k_3\cdot p_2)^a}\,, \tag{2.19}$$

$$\mathcal{S}_{32}^{(1)} = \frac{(k_3\cdot p_1)^a (k_3\cdot p_2)^a}{(k_3\cdot k_1)^a (k_3\cdot k_2)^a + (k_3\cdot p_1)^a (k_3\cdot p_2)^a}\,, \tag{2.20}$$

equations (2.10)–(2.15) are fulfilled ($i \equiv 3$, the gluon being the FKS parton). In eqs. (2.19) and (2.20) a is an *arbitrary* positive real number; the physical results will not depend on a, and their stability against the variation of a will constitute a check of the correctness of our implementation. It is clear that the numerators of eqs. (2.19) and (2.20) will act as damping factors for final- and initial-state collinear singularities respectively; the larger a, the stronger the damping. Formally, in the $a \to \infty$ limit we could recover the Θ-based implementation of the $\mathcal{S}$ functions of refs. [17, 18]. More pragmatically, we shall use the freedom in the choice of a to improve, if necessary, the numerical stability of the result, and will study its impact on the number of negative-weight events in MC@NLO, see section 4.

We now turn to the case of process (2.7); the corresponding Feynman diagrams are shown in fig. 3. There are only initial-state collinear singularities in this case, due to the splittings $g \to b\bar{b}$ (graph 2) and $g \to d\bar{d}$ (graph 3). On the other hand,

[4]It is immediate to see that the procedure adopted here to disentangle the singularities of $(\alpha, \beta; t, \gamma, \delta)$ works identically for $(\beta, \alpha; t, \gamma, \delta)$.

these two diagrams do not interfere: the former contributes to the t-channel cross section, the latter to the s-channel one. Since s- and t-channel contributions are integrated separately, we are in the same situation as process (2.4) (i.e., only one parton can give singularities), except for the fact that no final-state singularities are present in this case. Therefore, we can set $\mathcal{S}^{(1)} = 0$ here, which implies $\mathcal{S}^{(0)} = 1$. It also implies that we are in the same situation as that treated in **I** (which also applies to many other processes implemented in MC@NLO). This situation now naturally appears as a particular case of a more general implementation in which singularities are disentangled by means of $\mathcal{S}$ functions.

Since process (2.8) is completely analogous to process (2.7), we finally deal with process (2.9), whose Feynman diagrams are shown in fig. 4. Of those, graphs 1 and 4 contribute to the Wt mode, which has not been considered here and are therefore dropped, while graphs 2 and 3 contribute to the t-channel. Graph 2 (graph 3) is singular when the $\bar{u}$ (d) is emitted collinearly to the initial-state gluon; since the two diagrams do interfere, we disentangle the singularities by means of the $\mathcal{S}$ functions. We assign the momenta according to

$$(b, g; t, d, \bar{u}) \,, \tag{2.21}$$

and we define

$$\mathcal{S}_2^{(0)} = \frac{(k_3 \cdot p_1)^a (k_3 \cdot p_2)^a}{(k_2 \cdot p_1)^a (k_2 \cdot p_2)^a + (k_3 \cdot p_1)^a (k_3 \cdot p_2)^a} \,, \tag{2.22}$$

$$\mathcal{S}_3^{(0)} = \frac{(k_2 \cdot p_1)^a (k_2 \cdot p_2)^a}{(k_2 \cdot p_1)^a (k_2 \cdot p_2)^a + (k_3 \cdot p_1)^a (k_3 \cdot p_2)^a} \,, \tag{2.23}$$

which again fulfill equations (2.10)–(2.15). Although the same arbitrary parameter a as in eqs. (2.19) and (2.20) has been used here, this is in fact not necessary; we could introduce another free parameter, independent of a.

We conclude this section by stressing that the functional dependences of the $\mathcal{S}$ functions given above are correlated with the momentum assignments chosen for the corresponding subprocesses. For example, eqs. (2.22) and (2.23) imply that the FKS parton will have four-momentum k_2 and k_3 respectively. Clearly, the subtraction formalism is independent of the particular labeling adopted for each process. Therefore, through a relabeling we can always assign four-momentum k_3 to the FKS parton. Such relabeling is a purely formal trick to render manifest the local matching between NLO matrix elements and MC subtraction terms.

As far as processes (2.4)–(2.6) are concerned, we pointed out before that only the gluon can play the role of FKS parton. Thus, the momentum assignment in eq. (2.18) and the analogous ones

$$(u, b; t, d, g) \tag{2.24}$$

$$(b, \bar{d}; t, \bar{u}, g) \tag{2.25}$$

are what we want; as a consequence, the $\mathcal{S}$ functions have still the forms given in eqs. (2.19) and (2.20). For the process in eq. (2.7), see fig. 3, we noted that in the cases of s- and t-channel contributions the singularities arise from the splittings $g \to d\bar{d}$ and $g \to b\bar{b}$ respectively. Therefore, we assign momenta as follows

$$(u, g; t, \bar{b}, d) \qquad s-\text{channel}, \tag{2.26}$$

$$(u, g; t, d, \bar{b}) \qquad t-\text{channel}, \tag{2.27}$$

and analogously for process (2.8)

$$(\bar{d}, g; t, \bar{b}, \bar{u}) \qquad s-\text{channel}, \tag{2.28}$$

$$(\bar{d}, g; t, \bar{u}, \bar{b}) \qquad t-\text{channel}. \tag{2.29}$$

Finally, owing to the fact that $\mathcal{S}_2^{(0)} \leftrightarrow \mathcal{S}_3^{(0)}$ when $k_2 \leftrightarrow k_3$, we write

$$\begin{aligned} \mathcal{M}^{(r)}(b, g; t, d, \bar{u}) &= \mathcal{S}_3^{(0)} \mathcal{M}^{(r)}(b, g; t, d, \bar{u}) + \mathcal{S}_2^{(0)} \mathcal{M}^{(r)}(b, g; t, d, \bar{u}) \\ &= \mathcal{S}_3^{(0)} \Big[\mathcal{M}^{(r)}(b, g; t, d, \bar{u}) + \mathcal{M}^{(r)}(b, g; t, \bar{u}, d) \Big]. \end{aligned} \tag{2.30}$$

In other words, we shall assign the momenta in process (2.9) in two different ways

$$(b, g; t, d, \bar{u})\,, \tag{2.31}$$

$$(b, g; t, \bar{u}, d)\,, \tag{2.32}$$

and for each of them we multiply the corresponding matrix element times $\mathcal{S}_3^{(0)}$ given in eq. (2.22); as shown in eq. (2.30), this is fully equivalent to eqs. (2.21)–(2.23).

As a final remark, we note that when keeping the same ordered notation (2.17) after charge conjugation the treatment of real emission corrections to anti-top production is perfectly analogous, and the inclusion of single-$\bar{t}$ requires no extra work.

2.2 MC cross sections expanded to NLO

As discussed in **I** and **II**, in order to construct the MC subtraction terms one needs the cross section obtained by keeping the first non-trivial order in the α_S expansion of the parton shower Monte Carlo that will be matched with the NLO computation. As in the previous papers, the explicit results presented here are relevant to HERWIG. The most general form of the MC cross sections is given in eq. (**II**.5.1), which we rewrite as follows

$$d\sigma\Big|_{\rm MC} = \sum_{\mu} \sum_{L} \sum_{l} d\sigma_\mu^{(L,l)}\Big|_{\rm MC}, \tag{2.33}$$

where the index μ generically indicates a collection of labels which unambiguously identify the $2 \to 3$ partonic subprocess. The index L assumes the values $+$, $-$, f_1, and f_2 (the latter two were denoted by Q and $\bar{Q}$ in **II**). The index l, which differs per colour structure, assumes the values $q_i{\cdot}q_j$, where q_i and q_j are the four-momenta of the colour partners relevant to the emission considered; in this way, the shower scale is

$$E_0^2 = |l| \equiv |q_i \cdot q_j| . \tag{2.34}$$

In **II** we had $l = s, t, u$ (and $E_0^2 = |l|/2$), but in the case of unequal masses this is not a convenient notation. Equations (**II**.5.2)–(**II**.5.5) are also unchanged apart from notation

$$d\sigma_\mu^{(+,l)}\Big|_{\rm MC} = \frac{1}{z_+^{(l)}} f_a^{(H_1)}(\bar{x}_{1i}/z_+^{(l)}) f_b^{(H_2)}(\bar{x}_{2i})\, d\hat{\sigma}_\mu^{(+,l)}\Big|_{\rm MC} d\bar{x}_{1i}\, d\bar{x}_{2i}\,, \tag{2.35}$$

$$d\sigma_\mu^{(-,l)}\Big|_{\rm MC} = \frac{1}{z_-^{(l)}} f_a^{(H_1)}(\bar{x}_{1i}) f_b^{(H_2)}(\bar{x}_{2i}/z_-^{(l)})\, d\hat{\sigma}_\mu^{(-,l)}\Big|_{\rm MC} d\bar{x}_{1i}\, d\bar{x}_{2i}\,, \tag{2.36}$$

$$d\sigma_\mu^{(f_1,l)}\Big|_{\rm MC} = f_a^{(H_1)}(\bar{x}_{1f}) f_b^{(H_2)}(\bar{x}_{2f})\, d\hat{\sigma}_\mu^{(f_1,l)}\Big|_{\rm MC} d\bar{x}_{1f}\, d\bar{x}_{2f}\,, \tag{2.37}$$

$$d\sigma_\mu^{(f_2,l)}\Big|_{\rm MC} = f_a^{(H_1)}(\bar{x}_{1f}) f_b^{(H_2)}(\bar{x}_{2f})\, d\hat{\sigma}_\mu^{(f_2,l)}\Big|_{\rm MC} d\bar{x}_{1f}\, d\bar{x}_{2f}\,, \tag{2.38}$$

where the flavours a and b of the incoming partons depend on the value of μ. The short-distance cross sections that appear on the r.h.s. of eqs. (2.35)–(2.38) can be read from eq. (**II**.5.6) and eq. (**II**.5.8)

$$d\hat{\sigma}_\mu^{(\pm,l)}\Big|_{\rm MC} = \frac{\alpha_{\rm S}}{2\pi} \frac{d\xi_\pm^{(l)}}{\xi_\pm^{(l)}} dz_\pm^{(l)} P_{a'b'}^{(0)}(z_\pm^{(l)})\, d\bar{\sigma}_{\mu'} \Theta\left((z_\pm^{(l)})^2 - \xi_\pm^{(l)} \right), \tag{2.39}$$

$$d\hat{\sigma}_\mu^{(f_\alpha,l)}\Big|_{\rm MC} = \frac{\alpha_{\rm S}}{2\pi} \frac{d\xi_{f_\alpha}^{(l)}}{\xi_{f_\alpha}^{(l)}} dz_{f_\alpha}^{(l)} P_{a'b'}^{(0)}(z_{f_\alpha}^{(l)})\, d\bar{\sigma}_{\mu'} \Theta\left(1 - \xi_{f_\alpha}^{(l)}\right) \Theta\left(z_{f_\alpha}^{(l)} - \frac{m_\alpha}{E_0 \sqrt{\xi_{f_\alpha}^{(l)}}} \right), \tag{2.40}$$

where the Θ's account for HERWIG dead regions (see sect. 4.3 of **II**), and the flavours a', b', and the values of μ' can be determined by considering the possible collinear splittings of the corresponding NLO tree-level processes.

As in **II**, we use unbarred and barred symbols to denote quantities relevant to $2 \to 3$ and $2 \to 2$ processes respectively. The momentum assignments for the former are given in eq. (2.16), while for the latter we use

$$\alpha'(\bar{p}_1) + \beta'(\bar{p}_2) \longrightarrow t(\bar{k}_1) + \gamma'(\bar{k}_2)\,, \tag{2.41}$$

which we shorten in a way similar to eq. (2.17)

$$(\alpha', \beta'; t, \gamma')\,. \tag{2.42}$$

In MC cross sections expanded to NLO, $2 \to 2$ momenta (entering $d\bar{\sigma}$ on the r.h.s. of eqs. (2.39) and (2.40)) are obtained by means of a suitable projection of the corresponding $2 \to 3$ momenta. The exact form of the projection is specific to the parton shower MC matched to the NLO computation, and for HERWIG can be worked out as was done in **II**. Here, we need to extend the formulae given in **II**, in

	$(u,\bar{d};t,\bar{b})$	$(\bar{d},u;t,\bar{b})$
$(u,\bar{d};t,\bar{b},g)$	$\pm(\bar{p}_1\cdot\bar{p}_2); f_{1,2}(\bar{k}_1\cdot\bar{k}_2)$	
$(\bar{d},u;t,\bar{b},g)$		$\pm(\bar{p}_1\cdot\bar{p}_2); f_{1,2}(\bar{k}_1\cdot\bar{k}_2)$
$(u,g;t,\bar{b},d)$	$-(\bar{p}_1\cdot\bar{p}_2)$	
$(\bar{d},g;t,\bar{b},\bar{u})$		$-(\bar{p}_1\cdot\bar{p}_2)$
$(g,u;t,\bar{b},d)$		$+(\bar{p}_1\cdot\bar{p}_2)$
$(g,\bar{d};t,\bar{b},\bar{u})$	$+(\bar{p}_1\cdot\bar{p}_2)$	

Table 1: Short-distance contributions to MC subtraction terms, for the s-channel. The two columns correspond to the two possible s-channel Born cross sections, distinguished by the direction of the incoming partons. For a given process, the entries show the emitting legs, and in round brackets the value of the shower scale E_0 (up to a sign), according to the possible colour flows.

	$(b,u;t,d)$	$(b,\bar{d};t,\bar{u})$
$(b,u;t,d,g)$	$+, f_1(\bar{p}_1\cdot\bar{k}_1);\ -, f_2(\bar{p}_2\cdot\bar{k}_2)$	
$(b,\bar{d};t,\bar{u},g)$		$+, f_1(\bar{p}_1\cdot\bar{k}_1);\ -, f_2(\bar{p}_2\cdot\bar{k}_2)$
$(b,g;t,d,\bar{u})$	$-(\bar{p}_2\cdot\bar{k}_2)$	
$(g,u;t,d,\bar{b})$	$+(\bar{p}_1\cdot\bar{k}_1)$	
$(b,g;t,\bar{u},d)$		$-(\bar{p}_2\cdot\bar{k}_2)$
$(g,\bar{d};t,\bar{u},\bar{b})$		$+(\bar{p}_1\cdot\bar{k}_1)$

Table 2: As in table 1, for the t-channel, with bu- and $b\bar{d}$-initiated Born processes.

	$(u,b;t,d)$	$(\bar{d},b;t,\bar{u})$
$(u,b;t,d,g)$	$+, f_2(\bar{p}_1\cdot\bar{k}_2);\ -, f_1(\bar{p}_2\cdot\bar{k}_1)$	
$(\bar{d},b;t,\bar{u},g)$		$+, f_2(\bar{p}_1\cdot\bar{k}_2);\ -, f_1(\bar{p}_2\cdot\bar{k}_1)$
$(u,g;t,d,\bar{b})$	$-(\bar{p}_2\cdot\bar{k}_1)$	
$(g,b;t,d,\bar{u})$	$+(\bar{p}_1\cdot\bar{k}_2)$	
$(\bar{d},g;t,\bar{u},\bar{b})$		$-(\bar{p}_2\cdot\bar{k}_1)$
$(g,b;t,\bar{u},d)$		$+(\bar{p}_1\cdot\bar{k}_2)$

Table 3: As in table 1, for the t-channel, with ub- and $\bar{d}b$-initiated Born processes.

order to treat the case of final-state partons with unequal masses; explicit results are given in appendix A.

As far as flavour combinations are concerned, it is simpler to read eqs. (2.39) and (2.40) from right to left, since this follows the logic which forms the basis of a parton shower. The MC starts with a Born-level ($2 \to 2$ for single-t production) process, and then lets each leg branch in all kinematically- and flavour-allowed configurations possible. This implies that several $2 \to 3$ processes may be generated starting from a given $2 \to 2$ process. We list all such processes explicitly in tables 1–3; the non-void entries give non-zero contributions to eq. (2.33). Thus, the index μ that classifies the $2 \to 3$ partonic processes can simply be chosen so as to count all of the quantities that appear in the first columns of the tables. Parton legs where the branchings occur are denoted by $+$, $-$, f_1, and f_2 (f_1 always coincides with the top quark); given the parton that branches, and the hard subprocess, a colour connection is established which fixes the shower scale E_0 unambiguously. The shower scales to be used in eqs. (2.39) and (2.40) are equal to the absolute values of the dot products listed in tables 1–3. We finally point out that the momentum assignments for the $2 \to 3$ processes in the tables above are the same as those adopted (after relabeling) in the context of the pure NLO computation. This puts the NLO and MC cross sections on the same footing from a notational viewpoint, which will be convenient for the formal manipulations to be carried out in the next section.

3. MC@NLO

The definition of the MC@NLO formalism is given in eq. (**I**.4.22) or eq. (**II**.2.1):

$$\begin{aligned}\mathcal{F}_{\rm MC@NLO} = \sum_\mu \int dx_1 dx_2 d\phi_3 \Bigg\{ & \mathcal{F}_{\rm MC}^{(3)} \left(\frac{d\overline{\Sigma}_\mu^{(f)}}{d\phi_3}\bigg|_{\rm ev} - \frac{d\overline{\Sigma}_\mu}{d\phi_3}\bigg|_{\rm MC} \right) \\ & + \mathcal{F}_{\rm MC}^{(2)} \Bigg[- \frac{d\overline{\Sigma}_\mu^{(f)}}{d\phi_3}\bigg|_{\rm ct} + \frac{d\overline{\Sigma}_\mu}{d\phi_3}\bigg|_{\rm MC} + \frac{1}{\mathcal{I}_2} \left(\frac{d\overline{\Sigma}_\mu^{(b)}}{d\phi_2} + \frac{d\overline{\Sigma}_\mu^{(sv)}}{d\phi_2} \right) \\ & + \frac{1}{\mathcal{I}_{\tilde{2}}} \left(\frac{d\overline{\Sigma}_\mu^{(c+)}}{d\phi_2 dx}\bigg|_{\rm ev} + \frac{d\overline{\Sigma}_\mu^{(c-)}}{d\phi_2 dx}\bigg|_{\rm ev} \right) - \frac{1}{\mathcal{I}_{\tilde{2}}} \left(\frac{d\overline{\Sigma}_\mu^{(c+)}}{d\phi_2 dx}\bigg|_{\rm ct} + \frac{d\overline{\Sigma}_\mu^{(c-)}}{d\phi_2 dx}\bigg|_{\rm ct} \right) \Bigg] \Bigg\}. \end{aligned} \tag{3.1}$$

There is a minor difference of notation with respect to eq. (**II**.2.1): the indices for the sum over all partonic processes are denoted in the present paper by μ, consistently with what was done in sect. 2.2. We refer the reader to **I** and **II** for all details relevant to the formalism. Single-t production is the first process implemented in MC@NLO in which *both* $\mathcal{S}_i^{(0)}$ and $\mathcal{S}_{ij}^{(1)}$ are non-zero for certain i and j. This has direct implications for eq. (3.1), which we now discuss.

As shown in sect. 2.2, for a given choice of the index μ which classifies the partonic processes the radiation pattern in the MC cross section is determined by the values of the indices L and l. On the other hand, the possible radiation patterns at the NLO level are determined by the $\mathcal{S}_i^{(0)}$ and $\mathcal{S}_{ij}^{(1)}$ functions. Inspection of sect. 2.1.2 and of tables 1–3 shows that, for a given μ, there are *at most* one $\mathcal{S}^{(0)}$ and one

$\mathcal{S}^{(1)}$ functions which are non-vanishing. Formally, this corresponds to defining two single-valued functions $i(\mu)$ and $j(\mu)$ such that $\mathcal{S}^{(0)}_{i(\mu)}$ and $\mathcal{S}^{(1)}_{i(\mu)j(\mu)}$ may be different from zero. This allows us to define the following quantities

$$\mathcal{S}^{(\mathrm{IN})}_{\mu} = \mathcal{S}^{(0)}_{i(\mu)}\,, \qquad \mathcal{S}^{(\mathrm{OUT})}_{\mu} = \mathcal{S}^{(1)}_{i(\mu)j(\mu)}\,, \tag{3.2}$$

where the labels IN and OUT are to remind us that $\mathcal{S}^{(0)}_{i}$ and $\mathcal{S}^{(1)}_{ij}$ select kinematics configurations relevant to initial- and final-state collinear emissions respectively. Note that one of the functions in eq. (3.2) may be still be vanishing (which is the case for $\mathcal{S}^{(1)}$ in processes (2.31) and (2.32)), but there cannot be other non-vanishing $\mathcal{S}$ functions. In any case, from eqs. (3.2) and (2.10) we obtain

$$\mathcal{S}^{(\mathrm{IN})}_{\mu} + \mathcal{S}^{(\mathrm{OUT})}_{\mu} = 1 \qquad \forall\,\mu\,. \tag{3.3}$$

Note that, since we have exploited relabeling invariance to assign the four-momentum k_3 always to the FKS parton, we have $i(\mu) \equiv 3$. Furthermore, since the other massless final-state parton has four-momentum k_2, we also have $j(\mu) \equiv 2$. However, eq. (3.2) holds independently of relabeling invariance. Furthermore, it is clear that an analogous equation must hold for any kind of hard reaction, and not only for single-t production, as a direct consequence of the definition of the FKS partition.

The term $\overline{\Sigma}^{(f)}$ is proportional to the real-emission matrix elements (see eq. (**I**.4.12) and eq. (**I**.4.13)); thus, according to eq. (2.11), in eq. (3.1) we understand

$$\frac{d\overline{\Sigma}^{(f)}_{\mu}}{d\phi_3} = \mathcal{S}^{(\mathrm{IN})}_{\mu}\frac{d\overline{\Sigma}^{(f)}_{\mu}}{d\phi_3} + \mathcal{S}^{(\mathrm{OUT})}_{\mu}\frac{d\overline{\Sigma}^{(f)}_{\mu}}{d\phi_3} \tag{3.4}$$

$$= \mathcal{S}^{(\mathrm{IN})}_{\mu}\frac{d\overline{\Sigma}^{(f)}_{\mu}}{d\phi^{(\mathrm{IN})}_3} + \mathcal{S}^{(\mathrm{OUT})}_{\mu}\frac{d\overline{\Sigma}^{(f)}_{\mu}}{d\phi^{(\mathrm{OUT})}_3}\,, \tag{3.5}$$

where we have introduced two different *parametrizations* ($d\phi^{(\mathrm{IN})}_3$ and $d\phi^{(\mathrm{OUT})}_3$) of the three-body phase space $d\phi_3$, analogously to what is done in FKS in the context of pure NLO computations (see sect. 2.1.2). Their explicit forms, which are irrelevant in what follows, will be given in app. B.

In eq. (3.1) each point (x_1, x_2, ϕ_3) corresponds to a $2 \to 3$ kinematic configuration (called $\mathbb{H}$). In previous MC@NLO implementations, a definite $2 \to 2$ configuration (called $\mathbb{S}$) was chosen given (x_1, x_2, ϕ_3), according to a mapping $\mathcal{P}_{\mathbb{H}\to\mathbb{S}}$ whose form is dictated by HERWIG. The definition of such an unique mapping requires elaborate manipulations of the MC subtraction terms since, as shown in eq. (**II**.B.32) and eq. (**II**.B.33), initial- and final-state emissions would naturally lead to the definitions of two different mappings $\mathcal{P}^{(\mathrm{IN})}_{\mathbb{H}\to\mathbb{S}}$ and $\mathcal{P}^{(\mathrm{OUT})}_{\mathbb{H}\to\mathbb{S}}$. Following the same arguments as in app. B of **II**, we could implement single-t production using an unique $\mathcal{P}_{\mathbb{H}\to\mathbb{S}}$; as discussed there, however, this may degrade the numerical accuracy in the integration step and the unweighting efficiency. Furthermore, the two mappings $\mathcal{P}^{(\mathrm{IN})}_{\mathbb{H}\to\mathbb{S}}$ and $\mathcal{P}^{(\mathrm{OUT})}_{\mathbb{H}\to\mathbb{S}}$

are a perfect match to the FKS phase-space partition, which enters eq. (3.1) through eq. (3.5); the mapping $\mathcal{P}^{(\mathrm{IN})}_{\mathbb{H}\to\mathbb{S}}$ ($\mathcal{P}^{(\mathrm{OUT})}_{\mathbb{H}\to\mathbb{S}}$) can be naturally expressed in terms of the variables of $d\phi_3^{(\mathrm{IN})}$ ($d\phi_3^{(\mathrm{OUT})}$). In practice, we replace eq. (**I**.4.23) and eq. (**I**.4.24) with the following pairs of equations

$$I_{\mathbb{H}}^{(\mathrm{IN})} = \sum_\mu \int dx_1 dx_2 d\phi_3^{(\mathrm{IN})} \left(\mathcal{S}_\mu^{(\mathrm{IN})} \frac{d\overline{\Sigma}_\mu^{(f)}}{d\phi_3^{(\mathrm{IN})}}\bigg|_{\mathrm{ev}} - \frac{d\overline{\Sigma}_\mu^{(L=\pm)}}{d\phi_3^{(\mathrm{IN})}}\bigg|_{\mathrm{MC}} \right), \tag{3.6}$$

$$\begin{aligned} I_{\mathbb{S}}^{(\mathrm{IN})} = \sum_\mu \int dx_1 dx_2 d\phi_3^{(\mathrm{IN})} \Bigg[& - \mathcal{S}_\mu^{(\mathrm{IN})} \frac{d\overline{\Sigma}_\mu^{(f)}}{d\phi_3^{(\mathrm{IN})}}\bigg|_{\mathrm{ct}} + \frac{d\overline{\Sigma}_\mu^{(L=\pm)}}{d\phi_3^{(\mathrm{IN})}}\bigg|_{\mathrm{MC}} \\ & + \frac{\mathcal{S}_\mu^{(\mathrm{IN})}}{\mathcal{I}_2} \left(\frac{d\overline{\Sigma}_\mu^{(b)}}{d\phi_2^{(\mathrm{IN})}} + \frac{d\overline{\Sigma}_\mu^{(sv)}}{d\phi_2^{(\mathrm{IN})}} \right) + \frac{1}{\mathcal{I}_{\tilde{2}}} \left(\frac{d\overline{\Sigma}_\mu^{(c+)}}{d\phi_2^{(\mathrm{IN})} dx}\bigg|_{\mathrm{ev}} + \frac{d\overline{\Sigma}_\mu^{(c-)}}{d\phi_2^{(\mathrm{IN})} dx}\bigg|_{\mathrm{ev}} \right) \\ & - \frac{1}{\mathcal{I}_{\tilde{2}}} \left(\frac{d\overline{\Sigma}_\mu^{(c+)}}{d\phi_2^{(\mathrm{IN})} dx}\bigg|_{\mathrm{ct}} + \frac{d\overline{\Sigma}_\mu^{(c-)}}{d\phi_2^{(\mathrm{IN})} dx}\bigg|_{\mathrm{ct}} \right) \Bigg], \end{aligned} \tag{3.7}$$

and

$$I_{\mathbb{H}}^{(\mathrm{OUT})} = \sum_\mu \int dx_1 dx_2 d\phi_3^{(\mathrm{OUT})} \left(\mathcal{S}_\mu^{(\mathrm{OUT})} \frac{d\overline{\Sigma}_\mu^{(f)}}{d\phi_3^{(\mathrm{OUT})}}\bigg|_{\mathrm{ev}} - \frac{d\overline{\Sigma}_\mu^{(L=f_{1,2})}}{d\phi_3^{(\mathrm{OUT})}}\bigg|_{\mathrm{MC}} \right), \tag{3.8}$$

$$\begin{aligned} I_{\mathbb{S}}^{(\mathrm{OUT})} = \sum_\mu \int dx_1 dx_2 d\phi_3^{(\mathrm{OUT})} \Bigg[& - \mathcal{S}_\mu^{(\mathrm{OUT})} \frac{d\overline{\Sigma}_\mu^{(f)}}{d\phi_3^{(\mathrm{OUT})}}\bigg|_{\mathrm{ct}} + \frac{d\overline{\Sigma}_\mu^{(L=f_{1,2})}}{d\phi_3^{(\mathrm{OUT})}}\bigg|_{\mathrm{MC}} \\ & + \frac{\mathcal{S}_\mu^{(\mathrm{OUT})}}{\mathcal{I}_2} \left(\frac{d\overline{\Sigma}_\mu^{(b)}}{d\phi_2^{(\mathrm{OUT})}} + \frac{d\overline{\Sigma}_\mu^{(sv)}}{d\phi_2^{(\mathrm{OUT})}} \right) \Bigg], \end{aligned} \tag{3.9}$$

in such a way that the total rate is now

$$\sigma_{tot} = I_{\mathbb{S}}^{(\mathrm{IN})} + I_{\mathbb{H}}^{(\mathrm{IN})} + I_{\mathbb{S}}^{(\mathrm{OUT})} + I_{\mathbb{H}}^{(\mathrm{OUT})}, \tag{3.10}$$

which replaces eq. (**I**.4.25). It should be clear that eqs. (3.6)–(3.9) are a direct consequence of the definition of MC@NLO: in fact, eq. (3.1) is recovered by inserting $\mathcal{F}_{\mathrm{MC}}^{(3)}$ on the r.h.s. of eqs. (3.6) and (3.8), and $\mathcal{F}_{\mathrm{MC}}^{(2)}$ on the r.h.s. of eqs. (3.7) and (3.9). We note that the Born ($\overline{\Sigma}^{(b)}$) and the soft-virtual ($\overline{\Sigma}^{(sv)}$) contributions have been manipulated similarly to what was done for the real-emission contribution in eq. (3.5); although strictly speaking this is not necessary, since these terms are finite and therefore not involved in any subtraction, it helps to improve the numerical evaluations of the integrals $I_{\mathbb{S}}^{(\mathrm{IN})}$ and $I_{\mathbb{S}}^{(\mathrm{OUT})}$. On the other hand, the remainders of the initial-state collinear subtraction ($\overline{\Sigma}^{(c\pm)}$) only appear in $I_{\mathbb{S}}^{(\mathrm{IN})}$, since $I_{\mathbb{S}}^{(\mathrm{OUT})}$ is associated with final-state emissions. We have also introduced two two-body phase-space parametrizations $d\phi_2^{(\mathrm{IN})}$ and $d\phi_2^{(\mathrm{OUT})}$, which are analogous to their three-body counterparts. Finally, we have introduced the notation

$$\overline{\Sigma}_\mu\Big|_{\mathrm{MC}} = \overline{\Sigma}_\mu^{(L=\pm)}\Big|_{\mathrm{MC}} + \overline{\Sigma}_\mu^{(L=f_{1,2})}\Big|_{\mathrm{MC}}, \tag{3.11}$$

which is the analogue of eq. (3.5) for MC subtraction terms. The first and second terms on the r.h.s. of eq. (3.11) receive contributions from eq. (2.39) and (2.40) respectively (i.e. from initial-state and final-state branchings). Taking into account the properties of the MC subtraction terms (see app. B), this implies that eqs. (3.6)–(3.9) are finite; in fact, final-state singularities of real-emission matrix elements and their corresponding counterterms are removed in eqs. (3.6) and (3.7) by $\mathcal{S}^{(\text{IN})}$, while initial-state singularities are removed in eqs. (3.8) and (3.9) by $\mathcal{S}^{(\text{OUT})}$. Thus, the same procedure as in sect. 4.5 of **I** can be used in order to generate the hard events that are given to the parton shower as initial conditions.

As a concluding remark, we point out that the reason why the subtraction formalism of refs. [17, 18] appears to be particularly well suited for MC@NLO implementations can be read from eqs. (3.6)–(3.9). The partition of the phase space into collinear-like singular regions gives the FKS parton the same role as the softest parton emitted by an MC in the first branching after the generation of the hard process. Since as explained in **I** and **II** the first branching is the only one that matters for matching the MC with an NLO computation, the FKS parton and the softest parton emerging from the first branching in the shower are naturally paired in the definition of MC@NLO. Apart from guaranteeing the local cancellation of IR singularities, such pairing also allows a good control on the numerical stability of the result. It is also important to recall that, in each of the IR singular regions defined by the FKS partition, there are no unnecessary NLO subtractions: the only counterterm contributing to the result is that relevant to the real matrix element singularity present in that given region. This fact is very beneficial in reducing the number of negative-weight events.

4. Results

In this section we present sample results for single-t production at the Tevatron with $\sqrt{S} = 1.96$ TeV. We limit ourselves here to comparing MC@NLO predictions with those obtained with HERWIG and with an NLO code we have written according to the subtraction method of refs. [17, 18], as discussed in sect. 2.1.2. As a preliminary step, we have checked that our NLO results (with $\mu_{\text{R}} = \mu_{\text{F}} = m_t$) for the total rate and various t and $\bar{t}$ distributions are in excellent agreement with those of MCFM [9]. All of the predictions given in this section have been obtained by using the MRST2002 default PDF set [19], and by setting $m_t = 178$ GeV, which result in total rates equal to 1.045 pb and 0.406 pb for t- and s-channel respectively. We have rescaled HERWIG results to the NLO cross section, since we are only interested in the comparison of shapes in the case of standard MC's. Also, we have only considered here HERWIG results for the t-channel contribution; studies that also involve the s-channel will be shown in a forthcoming paper. All the MC@NLO and HERWIG results (but not, of course, the NLO ones) include the hadronization of the partons in the final state; furthermore, we forced the W emerging from the top decay to decay into a pair of leptons. In order to reduce as much as possible the statistical errors, we have generated $5 \cdot 10^5$ events for each MC@NLO and HERWIG run[5]. Finally, we stress that all of the fixed-order predictions presented here will be denoted as having NLO accuracy, even in the case of observables which, in the sense of perturbation theory, are effectively of leading order (see e.g. $p_{\mathrm{T}}^{(tj)}$ below); this is consistent with the terminology one *needs* to adopt in the context of MC@NLO (sect. 2.3 of **I**).

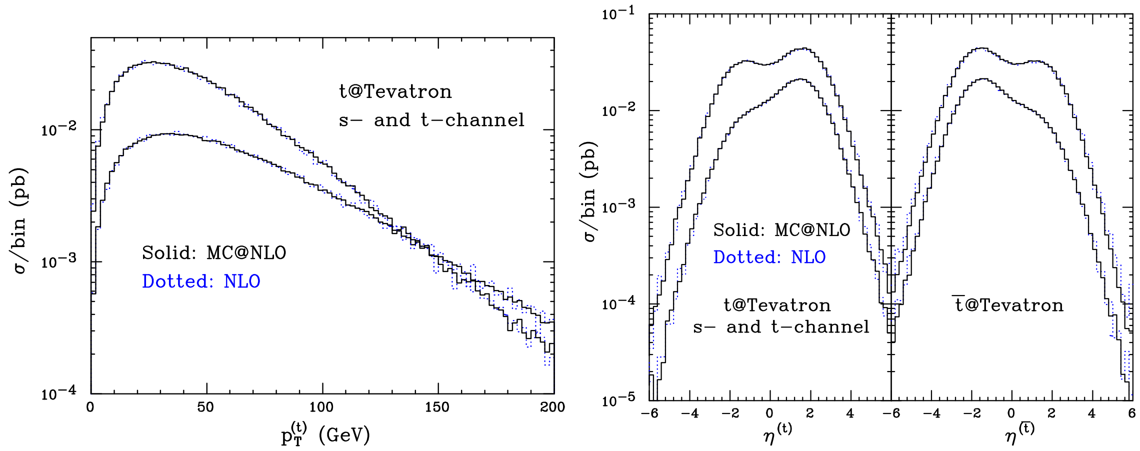

Figure 5: Comparison of MC@NLO (solid) and NLO (dotted) results. Left pane: top p_{T}, for t-channel (higher peak) and s-channel (lower peak) contributions. We have checked that $p_{\mathrm{T}}^{(t)} = p_{\mathrm{T}}^{(\bar{t})}$. Right pane: top (left) and antitop (right) η, for t-channel (higher curves) and s-channel (lower curves) contributions.

We start by considering the transverse momentum and pseudorapidity of the top and antitop (see fig. 5). We expect the impact of the momentum reshuffling that takes place during the hadronization phase in MC@NLO to be negligible on such observables. We also expect these observables, being sufficiently inclusive, to be reliably predicted by pure-NLO computations. As we see from the figure, the good agreement between MC@NLO and NLO confirms our expectations, and suggests that NNLO effects should be small. We have found that the HERWIG results are extremely close to the MC@NLO ones, and for this reason are not shown on the plots. As for all other processes previously studied, we have observed a much-improved behaviour from the numerical point of view when going from NLO to MC@NLO predictions, which is due to the fact that in MC@NLO all cancellations between large numbers occur at the level of short-distance cross sections, rather than in histograms as in the case of NLO computations. It is reassuring to see that this property holds true also

[5]Clearly, we are not suggesting to collect an integrated luminosity of $\mathcal{O}(1)$ ab^{-1} at the Tevatron. Here, we simply aim to expose the features of the two MC simulations with some precision.

for single-t production, which is the most involved process treated so far because of the simultaneous presence of initial- and final-state collinear singularities.

We now discuss the properties of a few jet observables. For the sake of clarity, we limit ourselves in this discussion to considering t-channel top events. We reconstruct the jets by means of the k_T-clustering algorithm [20], with $d_{cut} = 100\ \mathrm{GeV}^2$. We include in the clustering procedure all final-state stable hadrons[6] and photons. After the jets are reconstructed, we throw away the one that contains the b-flavoured hadron whose parent parton is the b quark emerging from top decay, and order the remaining ones in transverse energy, i.e. the hardest jet is the one with the largest E_T.

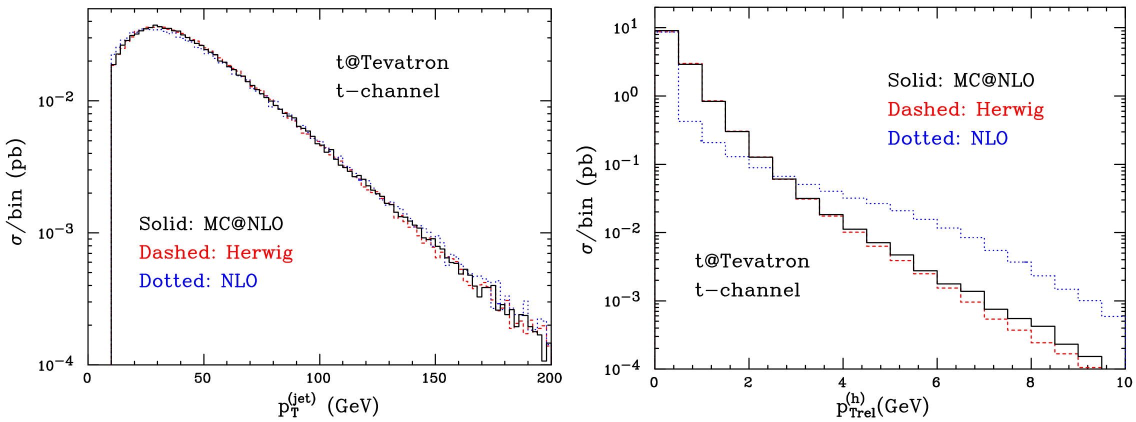

Figure 6: MC@NLO (solid), HERWIG (dashed), and NLO (dotted) results, for the p_T of the hardest jet (left pane), and the p_T relative to the axis of the hardest jet of those hadrons or partons in that jet (right pane).

We recall that we do not let the top decay in our pure-NLO computation. Also, we expect that some of the partons resulting from the radiation by the b quark emerging from the top decay in MC@NLO and HERWIG will hadronize into hadrons that are not clustered into the b-jet which we throw away. Furthermore, some extra radiation will occur from the top line due to showering, which is not included in the NLO computation. Finally, those jets obtained with MC@NLO and HERWIG are at the hadron level, while those obtained with the NLO computation are at the parton level.

In spite of these differences, there is a good agreement between MC@NLO, HERWIG, and NLO for the p_T of the hardest jet, shown in the left pane of fig. 6. This observable is sufficiently inclusive for this to happen, and the small differences between MC@NLO and NLO at small p_T are mainly due to the hadronization phase. On the other hand, the internal structure of the jet is very different in MC@NLO

[6]For the sake of simplicity, we force π^0's and all lowest-lying b-flavoured states to be stable in HERWIG.

and HERWIG from that resulting from the NLO computation. In the right pane of fig. 6 we present the transverse momentum, relative to the axis of the jet, of all of the hadrons or partons clustered into the jet itself. At the NLO, the jet often coincides with a single parton, hence the sharp peak at $p_{\mathrm{Trel}}^{(h)} = 0$. Such a peak is much less pronounced in the case of the MC's, since in those cases the jet almost never coincides with a single hadron. On the other hand, at large $p_{\mathrm{Trel}}^{(h)}$ the MC results are smaller than the NLO one: this must be so, since in the final states obtained with MC simulations it is likely that a large-$p_{\mathrm{Trel}}^{(h)}$ hadron will be clustered into another jet. This is much less probable at the NLO, simply because the number of jets there is limited to two. It is also interesting to observe that, although very small, the effect of the hard emissions due to the NLO real matrix elements is visible in the tail of the $p_{\mathrm{Trel}}^{(h)}$ distribution, the MC@NLO result being slightly harder than the HERWIG one.

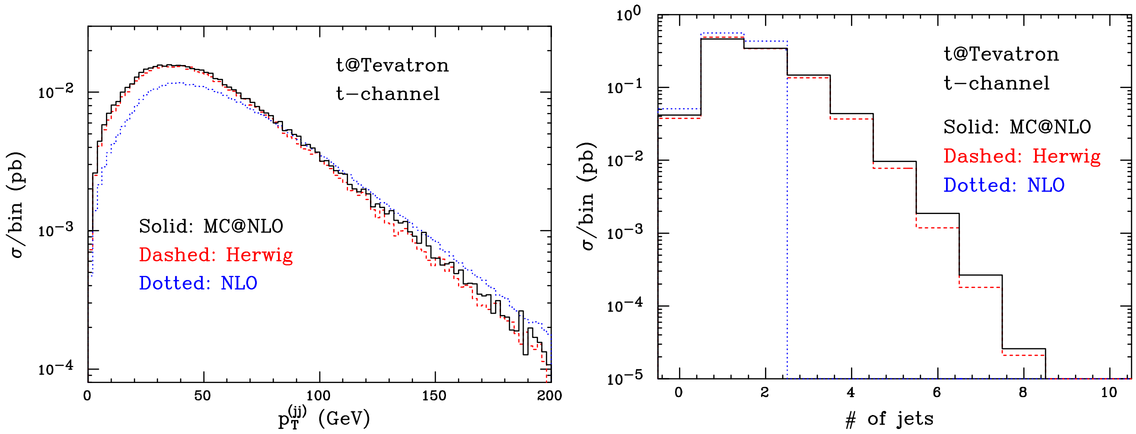

Figure 7: As in fig. 6, for the p_{T} of the two-hardest-jet pair (left pane), and for the number of jets (right pane).

The differences between the topologies of the final states emerging from NLO computations and MC@NLO and HERWIG simulations are clearly visible when we consider observables less inclusive than the p_{T} of the hardest jet. In the left pane of fig. 7 we plot the p_{T} of the pair of the two hardest jets. As is clear from the fact that MC@NLO and HERWIG have very similar shapes, which are different from the NLO one, the real matrix elements play a minor role here compared to the multiple emissions of the shower. The effects of the real matrix elements are more clearly visible in the tail of the distribution in the number of final-state jets (right pane of fig. 7), with MC@NLO predicting more events with more than two jets compared to HERWIG.

It is also interesting to observe that shower effects dominate over matrix element ones for top-hardest jet correlations, two of which we present in fig. 8. We stress again here that we did not make any systematic attempt to exclude from the jet

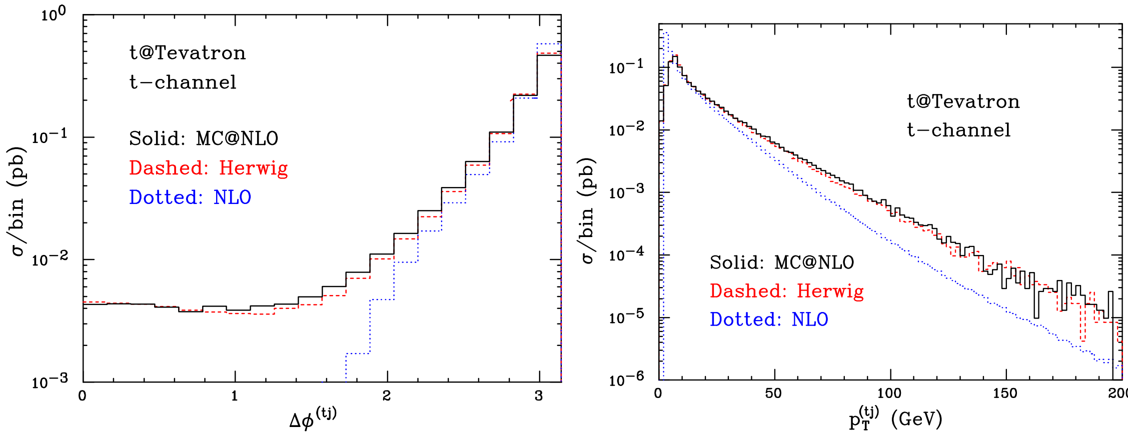

Figure 8: As in fig. 6, for the azimuthal difference between (left pane), and the p_{T} of (right pane) the top-hardest jet pair.

clustering the partons radiated by the top and its decay products, which would allow a closer matching between MC's and NLO results for these correlations. This is very clearly shown by the left pane of fig. 8, which presents the difference in azimuth between the top and the hardest jet. While the NLO prediction is zero for $\Delta\phi^{(tj)} < \pi/2$ for kinematics reasons (there is nothing in this region for the top-hardest jet pair to recoil against), MC@NLO and HERWIG feature a long tail which extends down to $\Delta\phi^{(tj)} = 0$. This is in part due to the fact that the top tends to have a much larger longitudinal than transverse momentum component. Thus, it is relatively easy for a parton, radiated by the top quark shower, to change the top transverse momentum by a sizable amount. The $\Delta\phi^{(tj)} = 0$ tail is mainly populated by such low-$p_{\mathrm{T}}^{(t)}$ events. In the right pane of fig. 8 we present the p_{T} of the top-hardest jet pair. At the NLO level, only $2 \to 3$ processes can contribute to the region $p_{\mathrm{T}}^{(tj)} \neq 0$, in the configurations in which the two final-state massless partons are not combined into a single jet; for this to happen, the two partons must be well separated. Clearly, such configurations imply the presence of a very off-shell intermediate particle, and are thus disfavoured by matrix elements: the $p_{\mathrm{T}}^{(tj)}$ distribution is steeply falling. In MC@NLO and HERWIG, $2 \to 3$ configurations result from a $2 \to 2$ hard process followed by a parton branching[7]. Since the branching is collinear in nature, the probability of getting two well-separated partons is even smaller than in NLO computations. However, the shower usually does not stop after the first branching. Furthermore, all strongly-interacting particles, including the top and the b emerging from the top decay, can radiate. This smears very effectively the final-state momenta; we have verified that, in the large-$p_{\mathrm{T}}^{(tj)}$ region, the hardest jet may retain a fraction of the parent parton momentum as small as 50%. This creates an imbalance between the top and the

[7]In MC@NLO, there are also $2 \to 3$ hard processes, whose matrix elements are the same as those of the NLO computation.

hardest-jet $p_{\rm T}$ which results in the much harder $p_{\rm T}^{(tj)}$ tails in MC@NLO and HERWIG relative to the NLO result. It should be stressed that such an effect is magnified by the steepness of the $p_{\rm T}^{(tj)}$ distribution. In terms of the total number of events, this is still a marginal phenomenon, which gives a negligible contribution to observables such as the inclusive $p_{\rm T}$ of the hardest jet. We conclude by observing again that the real matrix elements contributions are small but visible in the differences between MC@NLO and HERWIG in the intermediate $\Delta\phi^{(tj)}$ and large-$p_{\rm T}^{(tj)}$ regions.

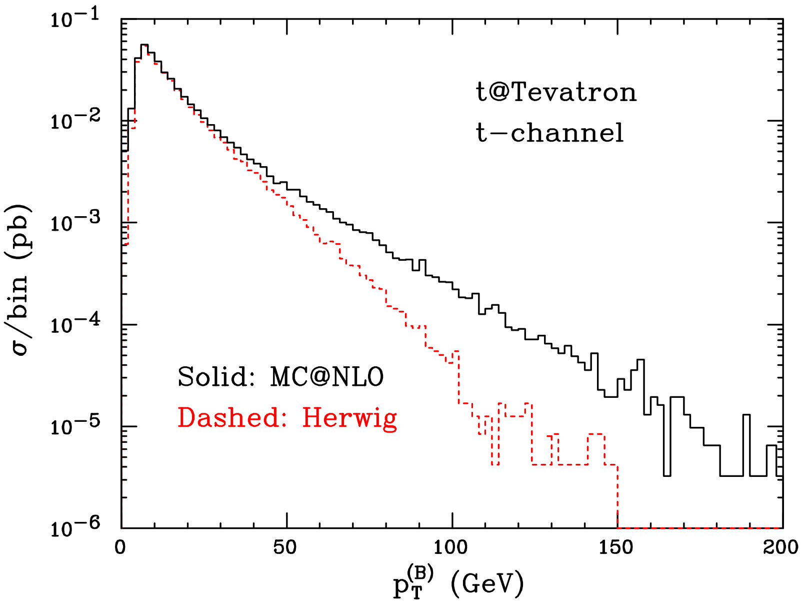

Figure 9: MC@NLO (solid) and HERWIG (dashed) results for the $p_{\rm T}$ of the b-flavoured hadrons (except those from top decay).

The results presented so far have shown little or no difference between MC@NLO and HERWIG results as far as shapes are concerned. Although larger differences could be seen by imposing hard transverse momentum cuts, the fact remains that at the Tevatron the phase-space for hard radiation is fairly limited. There are, however, observables that are particularly sensitive to real matrix element effects, such as the transverse momentum of the b-flavoured hadrons[8], which we present in fig. 9. This is because in t-channel matrix elements a b quark is almost always present in the initial state (up to CKM-suppressed contributions). This results in a final-state b-flavoured hadron which, in the case of HERWIG, acquires its transverse momentum entirely through the backward evolution in the shower mechanism. Such a mechanism is also present in MC@NLO, but there are also NLO real matrix elements in which a b quark has a large $p_{\rm T}$, which is inherited by the resulting b-flavoured hadron, and

[8] b-flavoured hadrons from top decay are not included in this plot.

which explains the difference in the large-$p_{\mathrm{T}}^{(B)}$ tail between MC@NLO and HERWIG[9].

We conclude this section by mentioning the fact that we observe no dependence (within the statistical accuracy of the runs we performed) of the physical results upon the unphysical parameters which enter the NLO subtraction formalism, such as the subtraction parameters introduced in refs. [17, 18], or the exponent a introduced in eqs. (2.19) and (2.20). This constitutes a test of the correctness of our implementation, since NLO results based on subtraction techniques are by construction independent of these parameters. Similarly, no dependence has been found on the parameters α and β introduced in eq. (**I**.A.86) and eq. (**I**.A.87) which control the behaviour of the MC subtraction terms in the soft limit, if they are restricted to their natural ranges ($\alpha = \mathcal{O}(1)$, $\beta = \mathcal{O}(0.1)$). This is as expected, since variation of these parameters gives only power-suppressed effects. On the other hand, all of the above parameters do affect the number of negative-weight events, and their tuning can be used to limit the presence of such events (whose fraction is equal to about 15% in the results presented here). The parameter a has only a limited impact on the number of negative weights (which change by about 1% for $1 \leq a \leq 4$), and its choice is mainly due to considerations of stability of the numerical integration, with best results for $a = 2$. In general, the accuracy of the predictions obtained with values of a larger than 2 (slowly) decreases with increasing a. Since the limit $a \to \infty$ corresponds to the Θ-based implementation of the subtraction formalism, this indirectly proves that the implementation introduced in this paper is more convenient from the numerical point of view.

5. Conclusions

In this paper we have considered single-top hadroproduction in the context of the MC@NLO approach. This case is, apart from its phenomenological relevance, also interesting from the technical point of view, since it features both initial- and final-state collinear singularities, and thus has a radiation pattern different from that of all of the processes so far included in MC@NLO.

We have shown that this is not a difficulty of principle, since the MC@NLO formalism is unchanged with respect to its definition given in ref. [14], but it entails a more involved procedure in the generation of the hard events that are given to the parton shower as initial conditions. Because this procedure is not specific to single-top hadroproduction, and since we have now treated all possible radiation patterns in MC@NLO, we are now in a position to include any new process, such as jet production, without the need of performing further analytical computations.

[9] For technical reasons, fig. 9 has been obtained by imposing $\left|y^{(B)}\right| < 3$. This cut has no impact for $p_{\mathrm{T}}^{(B)} > 10$ GeV.

As in previous cases, our computation is based on the universal subtraction formalism of refs. [17, 18]. We have used single-top hadroproduction as a test case, to explore an implementation of the subtraction different from that of the original papers. The partition of the phase space is now achieved by means of smooth functions of invariants, rather than with Θ functions as was done previously. This does not entail any change in the analytical formulae, but helps to improve the behaviour of the numerical computations. There is also a conceptual difference, namely that the infrared singularities are now disentangled by means of damping factors, rather than by non-overlapping regions defined by the phase-space partition. This in turn may lead to the possibility of implementing alternative subtraction schemes, although new analytical computations would be required in such a case.

We have not explored in this paper the phenomenological implications of our work, since we limited ourselves to checking that all of the observables we have considered show the expected behaviour in regions where the NLO computations or the MC simulations should be most reliable. We postpone the phenomenological studies, as well as the implementation of the Wt mode and spin correlations, to a forthcoming paper.

Acknowledgments

We would like to thank the CERN TH division for hospitality during the completion of this work. The work of E.L. and P.M. is supported by the Netherlands Foundation for Fundamental Research of Matter (FOM) and the National Organization for Scientific Research (NWO); that of B.W. is supported in part by the UK Particle Physics and Astronomy Research Council. The Feynman diagrams in the paper have been drawn using the Jaxodraw package [21].

A. Kinematics

In this section, we generalize the results of sect. 4 of **II** by considering the case of two final-state partons with unequal masses. Consistently with **II**, we use unbarred and barred symbols to denote quantities relevant to $2 \to 3$ and $2 \to 2$ processes respectively (see e.g. eqs. (2.16) and (2.41) for four-momentum assignments). Although in single-t production one of the final-state partons in $2 \to 2$ processes is massless, we shall derive our results in the most general case

$$\bar{k}_1^2 = m_1^2 \,, \qquad \bar{k}_2^2 = m_2^2 \,. \tag{A.1}$$

We start by defining the $2 \to 2$ reduced invariants as follows

$$\bar{s}_L = 2\bar{p}_1 \cdot \bar{p}_2 \,, \qquad \bar{t}_L = -2\bar{p}_1 \cdot \bar{k}_1 \,, \qquad \bar{u}_L = -2\bar{p}_1 \cdot \bar{k}_2 \,, \tag{A.2}$$

with $L=+,-,f_1,f_2$. These invariants are used in the computations of the Born cross sections which appear in the MC cross sections expanded to NLO, hence the dependence on the branching leg L in eq. (A.2). We also get

$$-2\bar{p}_2\cdot\bar{k}_2=\bar{t}_L+\Delta m_{12}^2\,,\qquad -2\bar{p}_2\cdot\bar{k}_1=\bar{u}_L-\Delta m_{12}^2\,, \tag{A.3}$$

where $\Delta m_{12}^2=m_1^2-m_2^2$. As discussed in **II**, the $2\to 2$ reduced invariants are functions of the invariants relevant to the $2\to 3$ kinematics. The computations required to determine such functions are non-trivial; we only report the results here:

$$\bar{s}_\pm=s+v_1+v_2\,, \tag{A.4}$$

$$\bar{s}_{f1,2}=s\,, \tag{A.5}$$

$$\bar{t}_\pm=-\frac{\bar{s}_\pm}{2}\left[1-\frac{x_2(t_1-u_1)+x_1(t_2-u_2)}{2s\sqrt{x_+^2-x_1x_2v_1v_2/s^2}}\right]-\frac{\Delta m_{12}^2}{2}\left(1+\frac{x_-}{\sqrt{x_+^2-x_1x_2v_1v_2/s^2}}\right), \tag{A.6}$$

$$\bar{t}_{f_1}=-\frac{1}{2}s\left[1-\left(\frac{t_2-u_1}{s-w_1}\right)\frac{\bar{\beta}}{\beta_2}\right]-\frac{1}{2}\Delta m_{12}^2\,, \tag{A.7}$$

$$\bar{t}_{f_2}=-\frac{1}{2}s\left[1-\left(\frac{t_1-u_2}{s-w_2}\right)\frac{\bar{\beta}}{\beta_1}\right]-\frac{1}{2}\Delta m_{12}^2\,, \tag{A.8}$$

$$\bar{u}_\pm=-\bar{s}_\pm-\bar{t}_\pm\,,\qquad \bar{u}_{f1,2}=-s-\bar{t}_{f1,2}\,, \tag{A.9}$$

where

$$\bar{\beta}=\sqrt{1-2\frac{\Sigma m_{12}^2}{\bar{s}}+\frac{\left(\Delta m_{12}^2\right)^2}{\bar{s}^2}}\,, \tag{A.10}$$

$$\beta_1=\sqrt{\left(1+\frac{\Delta m_{12}^2}{s-w_2}\right)^2-\frac{4sm_1^2}{(s-w_2)^2}}\,, \tag{A.11}$$

$$\beta_2=\sqrt{\left(1-\frac{\Delta m_{12}^2}{s-w_1}\right)^2-\frac{4sm_2^2}{(s-w_1)^2}}\,, \tag{A.12}$$

and $\Sigma m_{12}^2=m_1^2+m_2^2$. The $2\to 3$ invariants that appear on the r.h.s. of eqs. (A.4)–(A.9) are labelled as in **II**; their definitions are also reported here in table 4. Equations (A.2)–(A.12) give sufficient information, with tables 1–3, to compute the shower scales to be used in eqs. (2.39) and (2.40).

We finally summarize the formulae for HERWIG showering variables. The case of initial-state emissions is identical to that studied in **II**, the condition $m_1\neq m_2$ being irrelevant here. When parton 1 branches, the showering variables z_+ and ξ_+ are related to the invariants as in eq. (**II**.4.31) and eq. (**II**.4.32):

$$v_1=-2\frac{1-z_+}{z_+^2}\xi_+E_0^2\,, \tag{A.13}$$

$$-\frac{v_2}{s}=\frac{1}{2}(1-z_+)(2-\xi_+)\,. \tag{A.14}$$

Label	Invariant	Relation
s	$2p_1 \cdot p_2$	
t_1	$-2p_1 \cdot k_1$	
t_2	$-2p_2 \cdot k_2$	
u_1	$-2p_1 \cdot k_2$	
u_2	$-2p_2 \cdot k_1$	
v_1	$-2p_1 \cdot k_3$	$-s - t_1 - u_1$
v_2	$-2p_2 \cdot k_3$	$-s - t_2 - u_2$
w_1	$2k_1 \cdot k_3$	$s + t_2 + u_1 - m_1^2 + m_2^2$
w_2	$2k_2 \cdot k_3$	$s + t_1 + u_2 + m_1^2 - m_2^2$
M_{12}^2	$(k_1 + k_2)^2$	$s + v_1 + v_2$

Table 4: Notation for $2 \to 3$ kinematics.

Using eq. (2.34) we can write the solutions explicitly:

$$z_+^{(l)} = \frac{2|\bar{l}|}{v_1}\left[1 - \sqrt{1 - \frac{v_1}{|\bar{l}|}\left(1 + \frac{v_2}{s}\right)}\right], \tag{A.15}$$

$$\xi_+^{(l)} = 2\left[1 + \frac{v_2}{s(1 - z_+^{(l)})}\right], \tag{A.16}$$

which are identical to eq. (**II**.4.33) and eq. (**II**.4.34) except for the different definition of the scale $\bar{l}$.

The branching of parton 2 will be described in terms of the variables z_- and ξ_-; these can be obtained from eqs. (A.13)–(A.16) by interchanging variables v_1 and v_2.

The formulae for final-state emissions are affected by the condition $m_1 \neq m_2$. When the parton with momentum k_1 branches, eq. (**II**.4.23) and eq. (**II**.4.24) still formally hold

$$w_1 = 2z_{f_1}(1 - z_{f_1})\xi_{f_1}E_0^2\,, \tag{A.17}$$

$$\zeta_{f_1} = (1 - z_{f_1})\frac{1 + (1 - z_{f_1}\xi_{f_1})/\tilde{\beta}_1}{1 + \tilde{\beta}_1}\,, \tag{A.18}$$

with

$$\tilde{\beta}_1 = \sqrt{1 - (w_1 + m_1^2)/E_0^2}\,, \tag{A.19}$$

$$\zeta_{f_1} = \frac{(2s - (s - w_1)\varepsilon_2)w_2 + (s - w_1)\left[(w_1 + w_2)\beta_2 - \varepsilon_2 w_1\right]}{(s - w_1)\beta_2\left[2s - (s - w_1)\varepsilon_2 + (s - w_1)\beta_2\right]}\,, \tag{A.20}$$

$$\varepsilon_2 = 1 - \frac{\Delta m_{12}^2}{s - w_1}\,. \tag{A.21}$$

It is apparent that eq. (A.20) coincides with eq. (**II**.4.27) when $m_1 = m_2$ (i.e. $\varepsilon_2 = 1$). Solving eqs. (A.19) and (A.20) we obtain

$$z_{f_1}^{(l)} = 1 - \tilde{\beta}_1 \zeta_{f_1} - \frac{w_1}{2(1+\tilde{\beta}_1)|\bar{l}|}\,, \tag{A.22}$$

$$\xi_{f_1}^{(l)} = \frac{w_1}{2z_{f_1}^{(l)}(1-z_{f_1}^{(l)})|\bar{l}|}\,, \tag{A.23}$$

which are identical to eq. (**II**.4.28) and eq. (**II**.4.29) except for the different definition of the scale $\bar{l}$.

The branching of the parton with momentum k_2 can be treated along the same lines. The showering variables $z_{f_2}^{(l)}$ and $\xi_{f_2}^{(l)}$ will be obtained from eqs. (A.22) and (A.23) by formally interchanging labels 1 and 2. Note that in this way the quantity ε_1 appears in the expression for ζ_{f_2}, and

$$\varepsilon_1 = 1 + \frac{\Delta m_{12}^2}{s - w_2}\,. \tag{A.24}$$

B. MC subtraction terms

In this section, we construct explicitly the MC subtraction terms for single-t production, expressing them in terms of the variables used in the NLO computation. In order to do this, we start by introducing the phase-space parametrizations used in ref. [17] to deal with initial- and final-state emissions; in both cases, we integrate out the trivial azimuthal angles. We have

$$d\phi_3^{(\text{IN})} = \frac{s}{1024\pi^4}\,\bar{\beta}\left((1-\xi_i)s\right)\,\xi_i\, d\xi_i dy_i d\cos\theta d\varphi\,, \tag{B.1}$$

$$d\phi_3^{(\text{OUT})} = \frac{s}{512\pi^4}\,\frac{\xi_j}{2-\xi_i(1-y_j)}\,\xi_i\, d\xi_i dy_i dy_j d\varphi_j\,, \tag{B.2}$$

where $\bar{\beta}(s)$ is given in eq. (A.10), and[10]

$$\xi_j = \frac{2(1-m_1^2/s-\xi_i)}{2-\xi_i(1-y_j)}\,. \tag{B.3}$$

The variables labelled with index i refer to the FKS parton (see eq. (**FKS**.4.3)), and those labelled with index j refer to the massless final-state parton that can become collinear to the FKS parton (see eq. (**FKS**.4.57)). Note that ξ_i is related to the variable x used in **I** and **II** by the following equation

$$x \equiv 1 - \xi_i\,. \tag{B.4}$$

[10]Since this section is specific to single-t production, we set $m_2 = 0$ here.

This implies that eq. (B.1) coincides with eq. (**II**.B.22). We rewrite the real-emission finite contributions to the single-t cross section (eq. (**FKS**.4.37) and eq. (**FKS**.4.65)) as follows:

$$d\sigma_i^{(in,f)} = \frac{1}{2}\left(\frac{1}{\xi_i}\right)_c \left[\left(\frac{1}{1-y_i}\right)_\delta + \left(\frac{1}{1+y_i}\right)_\delta\right] \left((1-y_i^2)\xi_i^2\mathcal{M}^{(r)}\right) \mathcal{S}_i^{(0)}\, d\tilde{\phi}_3^{(\mathrm{IN})}\,, \quad \text{(B.5)}$$

$$d\sigma_{ij}^{(out,f)} = \left(\frac{1}{\xi_i}\right)_c \left(\frac{1}{1-y_j}\right)_\delta \left((1-y_j)\xi_i^2\mathcal{M}^{(r)}\right) \mathcal{S}_{ij}^{(1)}\, d\tilde{\phi}_3^{(\mathrm{OUT})}\,, \quad \text{(B.6)}$$

where

$$d\phi_3^{(\mathrm{IN})} = \xi_i\, d\tilde{\phi}_3^{(\mathrm{IN})}\,, \qquad d\phi_3^{(\mathrm{OUT})} = \xi_i\, d\tilde{\phi}_3^{(\mathrm{OUT})}\,. \quad \text{(B.7)}$$

As discussed in **I** and **II**, MC subtraction terms can be obtained from the MC cross sections expanded to NLO. Thus, following eq. (**II**.B.21), in order to construct them we must write eq. (2.39) in the same form as eq. (B.5) (after relabeling), and eq. (2.40) in the same form as eq. (B.6) (after relabeling). In order to do this, we note that the Born cross sections that appear in the MC subtraction terms have the following forms (in order to simplify the notation, we neglect here most of the indices)

$$d\bar{\sigma} = \mathcal{M}^{(b)}(\bar{s}_\pm, \bar{t}_\pm)\, \frac{\bar{\beta}(\bar{s}_\pm)}{16\pi}\, d\cos\theta_{in}\,, \quad \text{(B.8)}$$

$$d\bar{\sigma} = \mathcal{M}^{(b)}(\bar{s}_{f_\alpha}, \bar{t}_{f_\alpha})\, \frac{\bar{\beta}(\bar{s}_{f_\alpha})}{16\pi}\, d\cos\theta_{out}\,, \quad \text{(B.9)}$$

for initial- and final-state branchings respectively. Here $\mathcal{M}^{(b)}$ is the Born matrix element, and the angles θ_{in} and θ_{out} have been introduced in eq. (**II**.B.32) and eq. (**II**.B.33) respectively. As discussed in **II**, it is not restrictive to obtain these scattering angles in the zero-angle-emission limits, which leads to

$$\theta_{in} = \theta\,, \qquad \theta_{out} = y_j\,, \quad \text{(B.10)}$$

where θ and y_j are integration variables in eqs. (B.1) and (B.2) respectively. The first relation in eq. (B.10) coincides with eq. (**II**.B.35). We also note that, in the zero-angle-emission limits, the (trivial) azimuthal angles generated by the showers can be chosen to coincide with the angles φ and φ_j of eqs. (B.1) and (B.2) for initial- and final-state branchings respectively. We shall therefore insert the factors $d\varphi/(2\pi)$ and $d\varphi_j/(2\pi)$ in eqs. (2.39) and (2.40). We rewrite eq. (2.39) as follows

$$d\hat{\sigma}^{(\pm)}\Big|_{\mathrm{MC}} = \frac{1}{(1-y_i^2)\xi_i}\,(1-y_i^2)\xi_i\, \frac{g_{\mathrm{S}}^2}{256\pi^4}\, \frac{P(z_\pm)}{\xi_\pm}\, \frac{\partial(\xi_\pm, z_\pm)}{\partial(\xi_i, y_i)}$$
$$\times\, \mathcal{M}^{(b)}(\bar{s}_\pm, \bar{t}_\pm)\, \Theta\left((z_\pm^{(l)})^2 - \xi_\pm^{(l)}\right) \bar{\beta}(\bar{s}_\pm)\, d\xi_i dy_i d\cos\theta d\varphi\,, \quad \text{(B.11)}$$

where the first factor on the r.h.s. matches the "event" part of eq. (B.5), i.e. that obtained by replacing the distributions with ordinary functions. Using eqs. (B.1) and (A.4), we get

$$\bar{\beta}(\bar{s}_\pm) d\xi_i dy_i d\cos\theta d\varphi = \frac{1024\pi^4}{s} d\tilde{\phi}_3^{(\mathrm{IN})}\,. \quad \text{(B.12)}$$

Therefore

$$
\left. d\hat{\sigma}^{(\pm)} \right|_{\rm MC} = \frac{1}{2\xi_i} \left[\frac{1}{1-y_i} + \frac{1}{1+y_i} \right] \left((1-y_i^2)\xi_i^2 \left. \frac{d\Sigma^{(L=\pm)}}{d\phi_3^{(\rm IN)}} \right|_{\rm MC} \right) d\tilde{\phi}_3^{(\rm IN)} , \quad \text{(B.13)}
$$

$$
\left. \frac{d\Sigma^{(L=\pm)}}{d\phi_3^{(\rm IN)}} \right|_{\rm MC} = \frac{4g_{\rm S}^2}{s} \frac{P(z_\pm)}{\xi_i \xi_\pm} \frac{\partial(\xi_\pm, z_\pm)}{\partial(\xi_i, y_i)} \mathcal{M}^{(b)}(\bar{s}_\pm, \bar{t}_\pm) \, \Theta \left((z_\pm^{(l)})^2 - \xi_\pm^{(l)} \right) , \quad \text{(B.14)}
$$

which is identical (up to notational differences) to eq. (**I**.A.72) and eq. (**I**.A.73). The MC subtraction terms that enter eq. (3.1) are readily obtained from eq. (B.14) using eq. (**I**.4.18):

$$
\left. \frac{d\overline{\Sigma}^{(L=\pm)}}{d\phi_3^{(\rm IN)}} \right|_{\rm MC} = \frac{\partial(\bar{x}_{1i}, \bar{x}_{2i})}{\partial(x_1, x_2)} \left. \frac{d\Sigma^{(L=\pm)}}{d\phi_3^{(\rm IN)}} \right|_{\rm MC} . \quad \text{(B.15)}
$$

The reduced Bjorken x's $\bar{x}_{1i}$ and $\bar{x}_{2i}$ are given in eq. (**II**.4.20) or eq. (**II**.4.22).

We now turn to the case of final-state emissions, and we rewrite eq. (2.40) as follows

$$
\begin{aligned}
\left. d\hat{\sigma}^{(f_\alpha)} \right|_{\rm MC} = {} & \frac{1}{(1-y_j)\xi_i} (1-y_j)\xi_i \frac{g_{\rm S}^2}{256\pi^4} \frac{P(z_{f_\alpha})}{\xi_{f_\alpha}} \frac{\partial(\xi_{f_\alpha}, z_{f_\alpha})}{\partial(\xi_i, y_j)} \mathcal{M}^{(b)}(\bar{s}_{f_\alpha}, \bar{t}_{f_\alpha}) \\
& \times \Theta \left(1 - \xi_{f_\alpha}^{(l)} \right) \Theta \left(z_{f_\alpha}^{(l)} - \frac{m_\alpha}{E_0 \sqrt{\xi_{f_\alpha}^{(l)}}} \right) \bar{\beta}(\bar{s}_{f_\alpha}) \, d\xi_i dy_i dy_j d\varphi_j . \quad \text{(B.16)}
\end{aligned}
$$

Using eq. (B.2) we get

$$
d\xi_i dy_i dy_j d\varphi_j = \frac{512\pi^4}{s} \frac{2 - \xi_i(1-y_j)}{\xi_j} d\tilde{\phi}_3^{(\rm OUT)} . \quad \text{(B.17)}
$$

Inserting this equation into eq. (B.16), and using eq. (A.5) we obtain

$$
\left. d\hat{\sigma}^{(f_\alpha)} \right|_{\rm MC} = \frac{1}{\xi_i} \frac{1}{1-y_j} \left((1-y_j)\xi_i^2 \frac{d\overline{\Sigma}^{(L=f_\alpha)}}{d\phi_3^{(\rm OUT)}} \right) d\tilde{\phi}_3^{(\rm OUT)} , \quad \text{(B.18)}
$$

$$
\begin{aligned}
\frac{d\overline{\Sigma}^{(L=f_\alpha)}}{d\phi_3^{(\rm OUT)}} = {} & \frac{2g_{\rm S}^2}{s} \frac{2 - \xi_i(1-y_j)}{\xi_i \xi_j} \bar{\beta}(s) \frac{P(z_{f_\alpha})}{\xi_{f_\alpha}} \frac{\partial(\xi_{f_\alpha}, z_{f_\alpha})}{\partial(\xi_i, y_j)} \mathcal{M}^{(b)}(s, \bar{t}_{f_\alpha}) \\
& \times \Theta \left(1 - \xi_{f_\alpha}^{(l)} \right) \Theta \left(z_{f_\alpha}^{(l)} - \frac{m_\alpha}{E_0 \sqrt{\xi_{f_\alpha}^{(l)}}} \right) . \quad \text{(B.19)}
\end{aligned}
$$

Note that we directly defined $\overline{\Sigma}$ (rather than Σ as in eq. (B.13)) thanks to eq. (**II**.4.7).

We have checked analytically that the MC counterterms introduced above locally cancel the collinear divergences of the real matrix elements. As already discussed in **I** and **II**, this happens in the soft limit only after angular integration. We therefore adopt here the same solutions as in eq. (**II**.B.43). As in the previous cases, we checked that the parametric dependence introduced in this way is totally negligible, as we expect from power-suppressed effects.

References

[1] P. Nason, S. Dawson and R. K. Ellis, *The total cross-section for the production of heavy quarks in hadronic collisions*, *Nucl. Phys.* **B303** (1988) 607.

[2] W. Beenakker, H. Kuijf, W. L. van Neerven and J. Smith, *QCD corrections to heavy quark production in $p\bar{p}$ collisions*, *Phys. Rev.* **D40** (1989) 54–82.

[3] P. Nason, S. Dawson and R. K. Ellis, *The one particle inclusive differential cross-section for heavy quark production in hadronic collisions*, *Nucl. Phys.* **B327** (1989) 49–92.

[4] W. Beenakker, W. L. van Neerven, R. Meng, G. A. Schuler and J. Smith, *QCD corrections to heavy quark production in hadron-hadron collisions*, *Nucl. Phys.* **B351** (1991) 507–560.

[5] B. W. Harris, E. Laenen, L. Phaf, Z. Sullivan and S. Weinzierl, *The fully differential single top quark cross section in next-to-leading order QCD*, *Phys. Rev.* **D66** (2002) 054024 [`hep-ph/0207055`].

[6] Z. Sullivan, *Understanding single-top-quark production and jets at hadron colliders*, *Phys. Rev.* **D70** (2004) 114012 [`hep-ph/0408049`].

[7] Z. Sullivan, *Angular correlations in single-top-quark and Wjj production at next-to-leading order*, *Phys. Rev.* **D72** (2005) 094034 [`hep-ph/0510224`].

[8] S. Zhu, *Next-to-leading order QCD corrections to $bg \to tW^-$ at the CERN Large Hadron Collider*, *Phys. Lett.* **B524** (2002) 283–288 [Erratum: *ibid* **B537** (2002) 351].

[9] J. Campbell, R. K. Ellis and F. Tramontano, *Single top production and decay at next-to-leading order*, *Phys. Rev.* **D70** (2004) 094012 [`hep-ph/0408158`].

[10] Q.-H. Cao and C. P. Yuan, *Single top quark production and decay at next-to-leading order in hadron collision*, *Phys. Rev.* **D71** (2005) 054022 [`hep-ph/0408180`].

[11] Q.-H. Cao, R. Schwienhorst and C. P. Yuan, *Next-to-leading order corrections to single top quark production and decay at Tevatron. 1: s-channel process*, *Phys. Rev.* **D71** (2005) 054023 [`hep-ph/0409040`].

[12] Q.-H. Cao, R. Schwienhorst, J. A. Benitez, R. Brock and C. P. Yuan, *Next-to-leading order corrections to single top quark production and decay at the Tevatron. 2: t-channel process*, *Phys. Rev.* **D72** (2005) 094027 [`hep-ph/0504230`].

[13] J. Campbell and F. Tramontano, *Next-to-leading order corrections to Wt production and decay*, *Nucl. Phys.* **B726** (2005) 109–130 [`hep-ph/0506289`].

[14] S. Frixione and B. R. Webber, *Matching NLO QCD computations and parton shower simulations*, *JHEP* **06** (2002) 029 [`hep-ph/0204244`].

[15] S. Frixione, P. Nason and B. R. Webber, *Matching NLO QCD and parton showers in heavy flavour production*, *JHEP* **08** (2003) 007 [`hep-ph/0305252`].

[16] S. Frixione and B. R. Webber, *The MC@NLO 3.1 event generator*, `hep-ph/0506182`.

[17] S. Frixione, Z. Kunszt and A. Signer, *Three-jet cross sections to next-to-leading order*, *Nucl. Phys.* **B467** (1996) 399–442 [`hep-ph/9512328`].

[18] S. Frixione, *A general approach to jet cross sections in QCD*, *Nucl. Phys.* **B507** (1997) 295–314 [`hep-ph/9706545`].

[19] A. D. Martin, R. G. Roberts, W. J. Stirling and R. S. Thorne, *Uncertainties of predictions from parton distributions. 1: Experimental errors*, *Eur. Phys. J.* **C28** (2003) 455–473 [`hep-ph/0211080`].

[20] S. Catani, Y. L. Dokshitzer, M. H. Seymour and B. R. Webber, *Longitudinally invariant k_T clustering algorithms for hadron-hadron collisions*, *Nucl. Phys.* **B406** (1993) 187–224.

[21] D. Binosi and L. Theussl, *JaxoDraw: A graphical user interface for drawing Feynman diagrams*, *Comput. Phys. Commun.* **161** (2004) 76–86 [`hep-ph/0309015`].